MAX-PLANCK-INSTITUT FÜR PLASMAPHYSIK

GARCHING BEI MÜNCHEN

ION DISSIPATION IN HIGH MACH NUMBER OBLIQUE SHOCKS

D. Biskamp, H. Welter

IPP VI/102 February 1972

Die nachstehende Arbeit wurde im Rahmen des Vertrages zwischen dem Max-Planck-Institut für Plasmaphysik und der Europäischen Atomgemeinschaft über die Zusammenarbeit auf dem Gebiete der Plasmaphysik durchgeführt.

IPP VI/102

D.Biskamp and
H. Welter

Ion Dissipation in High Mach number oblique shocks

February 1972
(in English)

Abstract

Numerical simulations have provided detailed information of the microscopic processes that occur in a high Mach-number oblique shock wave such as the bow shock. The gross feature of the ion dissipation is a strong interaction of the reflected ions with the whistler precursor, which can be explained by a nonlinear ion-ion counter-streaming instability. The instability simultaneously amplifies the magnetic oscillations of the whistler which supports the strong magnetic turbulence at the bow shock. In addition electrostatic substructures have been observed which significantly enhance the thermalization of the ion distribution on the Debye scale.

The essential point in the theory of collisionless shock waves is the nature of the dissipation. While much progress has been made in recent years in understanding the collective processes in subcritical shocks, the knowledge about what happens in the high-Mach-number regime is still limited. This is especially true for shock waves propagating obliquely with respect to the ambient magnetic field. The experimentitally best known example is the bow shock in front of the earth's magnetosphere which we shall always refer to in the following. Satellite measurements have provided rather detailed information on the structure of this shock transition (Fredricks at al., 1968 and 1970; Montgomery et al., 1970). The following properties are now well established: The main dissipation process is anomalous ion heating; the ion temperature, which is usually smaller than the electron temperature in the upstream state, becomes much larger than the electron temperature behind the shock transition. The magnetic field profiles are highly oscillatory in the neighborhood of the shock transition. There exsists a considerable level of high frequency turbulence which is essentially electrostratic.

Since single satellite measurements do not yield unambiguous information of wave lengths, experimental identification of the type of magnetic waves present in the bow shock is difficult. A widespread view is, that they are predominantly whistlers. Little is known about the excitation mechanism. It would be very satisfying if it were directly connected with the process of ion dissipation.

The electrostatic turbulence is generally interpreted as a microturbulence with $k \lambda_D \sim 1$. A possible mechanism of excitation was first suggested by Fredricks et al., 1968. Since the high frequency oscillations are often correlated with strong magnetic field gradients, i.e. high current densities (Fredricks et al.), they appear to be due to the same instability which produces turbulence and anomalous resistivity in laboratory collisionless shock waves. This instability is now quite well understood theoretically (Forslund et al., 1971). In contrast to the well known two-stream instability in an unmagnetized plasma, which requires a large temperature ratio T_e/T_i for drift velocities smaller than the electron thermal velocity v_{the}, the instability produced by a current perpendicular to a magnetic field exists almost independently of the temperature

ratio. This resistive mechanism will heat essentially the electrons. However, there may be other sources of electrostatic instabilities which could give rise to stronger ion dissipation.

Phenomenologically, the main dissipation in a high Mach number shock wave is due to ion viscosity, i.e. to some process involving only the ion component of the plasma. The problem is to find the dominant collisionless mechanism. This determines, for instance, the scale length of ion heating. Several different processes are conceivable some of which have been discussed previously. Thermalization may occur within an electrostatic subshock with a thickness of the order of the Debye length (Tidman, 1967; Lindman and Drummond, 1971; Bertotti et al., 1971); or it may be due to some instability involving also magnetic oscillations, which would give rise to a thermalization scale $\gtrsim c/\omega_{pe}$; or, finally, there may be no sufficiently strong instability in which case thermalization occurs only via ion gyration effects taking a distance longer than c/ω_{pi} (Auer et al., 1971). However, none of these ideas have yet been convincingly proved or disproved. This is due to the fact that, on the one hand, satellite observations have not furnished sufficient information of the microscopic processes involved in the bow shock, and, on the other, that present theoretical

methods such as linear stability analysis or weak turbulence theory are not reliable in describing the highly nonlinear processes in a supercritical shock wave.

A possibility of avoiding the shortcomings of pure theory is to use numerical methods i.e. to conduct some"computer experiment". Previous numerical computations of oblique shock waves (Rossow 1967, Lindman and Drummond 1971) were primarily based on the macroparticle model devised by Auer, Hurwitz and Kilb (1962) for a perpendicular shock wave. This model is well suited to describe subcritical, laminar shock waves. However, in the case of a supercritical wave the statistical noise introduced by the small number of simulation particles becomes very high, which makes the physical interpretation of the numerical results ambiguous. An alternative numerical method is the PIC (particle-in-cell) method (Birdsall and Fuss, 1969; Morse and Nielson, 1969), which in the last few years has become a very powerful tool for treating collisionless plasma phenomena. Using this method we have performed numerical simulations of high Mach-number oblique shocks. In section 2 we describe the numerical model and give the main results of the computations. Section 3 discusses the linear dispersion relation

for a magnetized plasma with counterstreaming ions beams, while in section 4 the nonlinear instability of two ion beams is investigated. In section 5 we compare the numerical results with measurements on the bow shock.

2) Numerical Simulations

The equations we investigate are the Vlasov equation for the electron and ion distribution functions and Maxwell's equations for the self-consistent electric and magnetic fields. Both electrons and ions are magnetized, and so we include the spatial scales c/ω_{pi} , c/ω_{pe} , c_A/ω_{pi} ($\sim \lambda_D$ for $\beta_e \sim 1$) , and the time scales Ω_i^{-1}, Ω_e^{-1}, ω_{pi}^{-1}, ω_{pe}^{-1}, where c_A is the Alfvén speed and $\beta_e = 8\pi n T_e / B^2$. To solve this system of equations numerically, we use the PIC-method: Electrons and ions are represented by a certain number N of simulation particles. They

~~They~~ move in a fixed grid of cells on which the macroscopic quantities, i.e. the densities and fields, are defined. At a time t_o the number of ions and electrons in the different cells and their mean velocities determine the charge density ρ and current density $\underline{j}$ in the centers of the cells. From ρ and $\underline{j}$ the electric and magnetic fields are computed and the particle velocities and positions are advanced in time to $t_o + \Delta t$ under the influence of these fields (for details of the PIC method see, for example, the review paper by Morse, 1970). The problem we treat, a plane oblique shock wave, is 1-dimensional in space, but 3-dimensional in velocity space. So we solve the equations

$$
\begin{aligned}
m_i \dot{\underline{v}}_j &= e\left(\underline{E} + \frac{1}{c}\,\underline{v}_j \times \underline{B}\right) \qquad \text{ions} \\
m_e \dot{\underline{v}}_j &= -e\left(\underline{E} + \frac{1}{c}\,\underline{v}_j \times \underline{B}\right) \qquad \text{electrons}
\end{aligned}
\qquad j = 1, \ldots, N \tag{1}
$$

together with Poisson's equation

$$
-\frac{d^2\phi}{dx^2} = 4\pi\rho \tag{2}
$$

and the equation for the vector potential

$$
-\frac{d^2\underline{A}_\perp}{dx^2} = \frac{4\pi}{c}\,\underline{j}_\perp . \tag{3}
$$

The perpendicular displacement current is neglected, which is consistent in one dimension. The coordinate system is indicated in Fig 1. The magnetic field has a component along the shock normal, B_x = const because of div $\underline{B}$ = o. We only briefly sketch the numerical procedure of solving equations (1) - (3), since it is very similar to the method C in the paper of Morse and Nielson (1971). Although the perpendicular canonical momentum is not conserved because of $B_x \neq$ o, it is very convenient to treat the x-component and the perpendicular components of Eqs.(1) in a different manner. The vector potential is written as $\underline{A}_\perp = \underline{A}_o + \underline{A}_1$, $\underline{A}_o$ = (o,o,$B_x y$) and $\underline{A}_1$ = (o, A_{1y}(x), A_{1z} (x)). Integrating the x-component of (1) gives the new particle positions from which ρ and ϕ can be computed.

The perpendicular part of (1) can be written in the form

(4) $$\dot{\underline{p}}_{\perp j} = \frac{e_j}{c}\underline{v}_{\perp j} \times \underline{B}_{\parallel} \,, \quad \underline{p}_{\perp j} \equiv m_j \underline{v}_{\perp j} - \frac{e_j}{c}\underline{A}_1 \,.$$

Integration of (4) gives $\underline{v}_{\perp}$, from which $\underline{j}$ and $\underline{A}_1$ are computed. The units chosen are c/ω_{pi}, Ω_i^{-1} (and hence c_A) and $B^2/4\pi n$ as energy unit, so that $T_{e,i} = 1/2\ \beta_{e,i}$. These quantities refer to the unperturbed plasma, i.e. the upstream state of the shock. Because of the different time and length scales involved in the present model, numerical feasibility imposes some restriction on the mass ratio and the parameter c/c_A.

The shock wave is generated by a constant electric field E_{oy} induced at the edge of the system, which drives a magnetic piston into the plasma. The general behaviour is illustrated in Fig. 2 showing a run with $\frac{mi}{me} = 128$, $T_e = 1/4$, $T_i = 1/16$, $c/c_A = 64$, (so that $c/\omega_{pi} = 128\,\lambda_D$), $E_{oy} = 20$ (measured in units $c_A/c\ B$) and $\Theta = 45^o$ (Θ = angle between magnetic field and shock normal). The wave front first steepens and a potential barrier is built up, until some of the ions are reflected. In a high Mach-number shock wave these reflected ions are the origin

of the anomalously high ion temperature, since both their energy and number rapidly increase with the Mach-number. The reflected ion beam then undergoes strong interaction with the whistler which is generated in front of the shock. They are trapped by the electric potential coupled to the whistler forming vortices in phase space (Fig. 2a). As these vortices are filled up, the actual shock front, characterized by the first particle reflecting potential hump, or more generally by the density profile, is moving upstream across the whistler, i.e. the shock speed, $M_A \simeq 5$, is somewhat higher than the phase velocity of the whistler, but not as high as the group velocity. At later times not shown in Fig.2., the downstream part of the whistler wave train is irreversibly damped as the density reaches its downstream value. The influence of the magnetic field on the ion dissipation is of minor importance. This has been demonstrated by repeating the same run with the Lorentz force of the ions switched off. No essential difference was observed, the ion phase space plots look similar to those of Fig. 1 a. Thus, we conclude that gyration effects of the reflected ion beam play no essential role in the thermalization process in the present run.

To further elucidate this beam-whistler interaction, we performed a number of runs varying the mass ratio, the driving field E_{oy}, and the parameter c/c_A. We first compare three runs with m_i/m_e= 64, 128, 256. To see more cearly the electrostatic trapping of the ions, the ions were taken to be unmagnetized in these runs.

Phase space plots are shown in Fig. 3. We find that the trapping process becomes more effective for larger mass ratio. In the case m_i/m_e = 64, Fig. 3a, only one phase space vortex is formed, while the main part of the reflected ions is flowing upstream nearly unperturbed. In the case m_i/m_e = 128, Fig. 3b, the interaction of the reflected ions with the incoming plasma is much stronger, two vortices have been formed at t = 2.25 Ω_i^{-1} , and only few particles are escaping upstream. For m_i/m_e = 256, Fig. 3c, this effect is still more pronounced. From the B-plots in Fig. 3 it is evident that the interaction of the reflected ions is correlated with the excitation of the whistler in front of the shock.

We then varied the Mach-number by changing the driving field E_{oy}. Increasing M_A reduces the strength of the electrostatic ion heating. This was shown by a run with the same parameter values as in Fig 2, but with E_{oy} = 32

which produces a shock wave with $M_A \simeq 5.8$. In this case only a single trapped ion vortex is formed most of the reflected ions following their gyro-orbits. In a further run we then increased the mass ratio, $m_i/m_e = 256$; the electrostatic interaction was again stronger in agreement with the dependence on the mass ratio illustrated in Fig.3. Varying the parameter c/c_A, i.e. the ratio $\frac{c}{\omega_{pi}}/\lambda_D$, no noticeable change of the gross features of the dissipation process was observed, since the wavelength is that of the whistler. However, superimposed on the large scale beam-whistler interaction are essentially electrostatic oscillations with wavelengths proportional to c_A/c, and hence to λ_D. This micro-turbulence is first excited in the regions of strong potential peaks, which correspond to electrostatic subshocks (Lindman and Drummond; Bertotti et al., 1971). Later on these regions broaden so that the electrostatic turbulence covers nearly the whole shock transition. It leads to an enhanced thermalization of the ion distribution function on the Debye scale. These feature can be recognized in Fig. 4, where ion phase space is plotted with higher spatial resolution than in Fig. 2. Here we selected a run with low initial ion temperature, $T_e/T_i = 25$, showing up the fine scale structures in phase space more clearly. Electrostatic subshocks have been

formed at $x \simeq 2.5$ and $x \simeq 4$, at a time $t = 1.5$ after one large trapping vortex, given in Fig. 2, has been formed.

To summarize the numerical results:

A strong interaction of the reflected ions with the whistler precursor has been observed which leads to ion trapping by the electric potential of the whistler. This interaction is weaker for higher Mach numbers but, on the other hand, becomes more effective with increasing mass ratio.Superimposed we find an electrostatic turbulence which plays an important part in the fine scale thermalization of the ion distribution function.

3) Linear Stability Analysis

It is natural to try and explain the ion dissipation observed in the numerical experiments in terms of an instability exited by the ions reflected from the shock front. The linear dispersion relation of a two-ion-beam plasma has been investigated previously by Bertotti and Biskamp (1969) in the purely electrostatic case and by Auer et al., (1971) and by Papadopoulos et al. (1971a) for two ion beams streaming perpendicular to a magnetic field. A common result of these studies is that in the two-ion-beam configuration the most unstable modes, i.e. those propagating in the direction of the beams, are stabilized when the relative drift velocity of the beams exceeds a critical value, $v_0 \simeq 2 c_s$, or in the presence of a perpendicular magnetic field $v_0 \simeq 2\sqrt{c_A^2 + c_s^2}$ (assuming $T_e \gg T_i$), where $c_s = \sqrt{T_e/m_i}$ is the ion-sound speed. Now the drift velocity between the incoming plasma and the reflected ions in a supercritical shock wave such as the bow shock is roughly $2 M_A c_A$, which is much larger than the critical velocity v_0 . Hence the conclusion was drawn by Auer et al. that ion heating does not occur via a strong instability but essentially by the gradual

thermalization of the reflected ion beam because of gyration. However these computations are restricted to the perpendicular case. One has still to consider the case of two ion beams streaming obliquely to a magnetic field (which is more adequate for bow shock conditions), where in fact the linear dispersion relation turns out to be quite different. In deriving this dispersion relation, we introduce the following simplifications: Both electrons and ions are treated in a fluid picture, i.e. wave-particle resonance effects are neglected. This is reasonable, since we are interested in the nonresonant interaction of the ion beams. Furthermore, the ions are assumed unmagnetized, which implies that the wavelengths of the modes investigated are smaller than the ion gyroradius $k\rho_i \sim k\, c/\omega_{pi} > 1$ and that the frequency and growth rate are larger than the ion gyrofrequency, $\omega, \gamma > \Omega_i$. On the other hand, $\omega < \Omega_e$, so that electron cyclotron resonances can be neglected. We choose the reference frame, where the plasma is in rest, $U_1 n_1 + U_2 n_2 = 0$, where n_1, n_2 are the density fractions of the beams and U_1, U_2 their velocities. Changes in the electron pressure are taken to be isothermal; however, assumption of a different law would

not change the dispersion relation qualitatively. Finally, we restrict ourselves to modes $\underline{k}$ parallel to the ion beams, since these modes have the strongest effect on the 2-ion beam configuration. In this case the dispersion relation becomes:

$$(5) \qquad \frac{n_1 \omega_{pi}^2}{(\omega - k u_1)^2} + \frac{n_2 \omega_{pi}^2}{(\omega - k u_2)^2} = 1 + \frac{1}{k^2 \lambda_D^2 + \sin^2\theta / G}$$

where

$$(6) \qquad G \equiv \frac{\omega_{pe}^2}{\Omega_e^2}\left(1 + \frac{\omega_{pe}^2}{k^2 c^2} - \frac{\Omega_e^2}{\omega^2}\frac{\cos^2\theta}{1 + \omega_{pe}^2/(kc)^2}\right)$$

is the dispersion function corresponding to the whistler branch and θ is the angle of $\underline{B}_o$ with respect to $\underline{k}$. The relation (5) was also obtained by Lindman and Drummond. In the bow shock and in most laboratory collisionless shock experiments one has $\Omega_e \sim \omega_{pi}$, so that $\omega_{pe}^2/\Omega_e^2 \gg 1$. In addition, we assume two equal density beams, $U_1 = -u_2 = u$ for convenience. For $k\lambda_D \sim 1$ (1) reduces to the simple nonmagnetic dispersion relation,

$$(3) \qquad \frac{\frac{1}{2}\omega_{pi}^2}{(\omega - ku)^2} + \frac{\frac{1}{2}\omega_{pi}^2}{(\omega + ku)^2} = 1 + \frac{1}{k^2\lambda_D^2} \; .$$

If $U > c_s$, the modes propagating along the beams are stable. Modes propagating at large angles with respect to the beam direction may still be unstable. However, their effect on the two ion beams is very small, as has been shown by 2-dimensional numerical simulation of this instability (Forslund and Shonk, 1970). For $k c/\omega_{pe} \lesssim 1$ and $\beta_e < 1$ Eq. (1) becomes:

$$(4)\quad \frac{\frac{1}{2}\omega_{pi}^2}{(\omega - kU)^2} + \frac{\frac{1}{2}\omega_{pi}^2}{(\omega + kU)^2} + \frac{\omega_{pe}^2}{\omega^2}\frac{\cot^2\theta}{1+\frac{\omega_{pe}^2}{k^2c^2}} = \frac{\omega_{pe}^2}{\sin^2\theta\,\Omega_e^2}\left(1+\frac{\omega_{pe}^2}{k^2c^2}\right).$$

Here the modes are no longer purely electrostatic. Magnetic field oscillations are coupled to electric potential oscillations. It is easy to obtain the instability threshold from Eq (4). The system is unstable if

$$(5)\quad 0 < kU < \frac{\Omega_e \cos\theta}{1+\frac{\omega_{pe}^2}{k^2c^2}} \quad .$$

For $\Omega_e \sim \omega_{pi}$ and $k c/\omega_{pe} \gtrsim 1$, $\cos\theta \sim 1$ Eq (4) predicts instability up to very high velocities, $U \lesssim \sqrt{m_i/m_e}\; c_A$. This instability, however, is <u>not</u> due to the interaction of the ion beams but is an

electron-ion instability with phase-velocities close to either ion beam. The ion - ion instability is suppressed by the high mobility of the electrons along the magnetic field, which is represented by the large third term on the left side of Eq (4). Even when $U < \sqrt{c_A^2 + c_S^2}$, which is the velocity range of the ion - ion beam instability in the perpendicular case, i.e. $\theta = \pi/2$, the ion - ion instability is not growing for beams oblique to the magnetic field.

The electron- ion instability given by Eq (4) has only very little effect nonlinearily, although its linear growth rate may be quite large. It is easily stabilized after heating the electrons and each separate ion beam somewhat. The free energy available in the ion - ion counterstreaming configuration is not used. This has been shown by following numerically the behaviour of a homogenous two-ion beam plasma using the particle model of section 2. Thus, we conclude that also in the more general case where the ion beams are streaming in some oblique direction with respect to the ambient magnetic field, no strong linear ion - ion instability exists under the conditions of a supercritical shock wave.

4) Nonlinear Two-Ion-Beam Instability

Though the two-ion beam configuration is linearly stable at high drift velocities, it constitutes a system far away from thermal equilibrium with a large content of free energy. By a sufficiently large perturbation a nonlinear instability may be triggered which transforms this energy into potential and thermal energy much in the same way as the linear instability does for small drift velocity of the beams.

We have investigated numerically the nonmagnetic one-dimensional two-ion beam configuration, varying the amplitude of the initial perturbation. We assume equal density beams, $n_1 = n_2$, with drift velocities $\pm u$, and high temperature ratio $T_e/T_i = 25$ to eliminate ion Landau damping. The main results are illustrated in Fig 4. For $u < c_s$ a linear instability starts out of the thermal noise, leading to rapid thermalization of the ion distribution (Fig 5a, $u = 0.75\, c_s$). For $u > c_s$ the system is linearly stable, even a small superthermal perturbation is not amplified (Fig 5b, $u = 3\, c_s$). However, modulation of the system by a wave with a sufficiently high amplitude ϕ_0 can trigger the instability, which subsequently evolves

similarly to the linear instability (Fig. 5 c, $U = 3\,c_s$, $e\phi_0 = 0.5\,T_e$). We also find that the amplitude necessary to initiate the instability increases as the relative drift velocity becomes larger.

We now identify the dissipation process in front of the shock wave with the effect of the ion - ion counterstreaming instability excited nonlinearly by the electric potential oscillations coupled to the whistler precursor (for oblique propagation the whistler is a mixed electrostatic - electromagnetic wave). This idea is supported by a number of arguments obtained from the numerical simulations. We have seen in section 2 that the ion trapping process becomes stronger with increasing mass ratio. The reason is that for larger mass ratio the whistler excitation in front of the shock is more effective because electron Landau damping becomes weaker which for $M_A c_A < v_{the}$ is proportional to $M_A\, c_A / v_{the} \sim \sqrt{m_e/m_i}$. Hence the instability can be triggered more easily. With increasing Mach-number the dissipation process becomes less effective. The reason is that the relative velocity between incoming and reflected ions becomes larger, which makes it more

difficult to excite the instability. In the case of a shock wave propagating perpendicularly to a magnetic field no anomalous dissipation of the reflected ion beam is observed. Assuming unmagnetized ions, the reflected ions are flowing upstream completely unperturbed, as has also been found by Forslund and Freidberg (1971) and Papadopulos et al. (1971 b). The reason is that in the perpendicular case no whistler precursor exists which could trigger the nonlinear instability.

5) Application to the bow shock

The interaction of the beam of reflected ions with the whistler precursor, as seen in the numerical simulations, can account for the rapid ion dissipation in the bow shock. It is coupled to strong excitation of whistler waves, which explains the very oscillatory magnetic structures at the bow shock. The rather regular magnetic field profiles seen in the computations seem to be essentially due to the one-dimensional character of the model. In three dimensions such coherent wave patterns will certainly be made turbulent by some wave-coupling process (see e.g. Wright, 1971). Also the thermalization process will probably be faster in higher dimensional systems. This effect is well known from two- and three-dimensional simulations of the 2-stream instability (Morse and Nielson, 1969). In addition to the large scale ion trapping by the whistler a significant level of electrostatic turbulence with $k\lambda_D \sim 1$ has been observed in our simulations. It is not localized at a certain point of the shock, i.e. there is no single, well defined electrostatic subshock, but a whole set of such subshocks, giving rise to a broad spatial range of the ion wave turbulence.

Thus we find that in addition to the current-driven turbulence, which as explained in the introduction, should play some role in the bow shock producing anomalous resistance, there is a second source of high frequency noise connected with the relaxaction of the reflected ions.
In our one-dimensional model the anomalous resistance is not contained. This implies that resistive electron heating is not included, which, however, is partly compensated by the artificially enhanced heating by electromagnetic whistler damping because of the small mass ratios used.

We have also seen in the computations that under certain conditions, especially at very high Mach numbers, the beam-whistler interaction may be reduced or completely suppressed. In this case bunches of reflected ions follow their gyro-orbits nearly unperturbed by electrostatic fluctuations. They form a high velocity beam which persists for a long time, until it becomes thermalized after many gyration. These particles may account for the secondary peaks in the ion distribution, especially in front of the shock, observed by Montgomery et al.

Conclusions:

We have presented numerical simulations of a one-dimensional oblique collision free shock wave in the Mach-number range of the bow shock. Using a shock model which includes electrostatic as well as electromagnetic interactions of both electrons and ions, we were able to describe processes of very different scales, ranging from c/ω_{pi} to λ_D. The main new feature observed was a strong interaction of the reflected ions with the incoming plasma, which we identified with a nonlinear ion-ion counterstreaming instability excited by the potential oscillations coupled to the whistler. This instability cannot be obtained by usual linear stability analysis. The thermalization is enhanced by small scale turbulence with $k\lambda_0 \sim 1$, excited in regions where the ion beams come close together. Occasionally, especially at very high Mach-numbers, may bunches of high energy ions escape the influence of the whistler potential humps and follow their gyro-orbits. These particles may give rise to the secondary peak in the ion distribution in front of the bow shock.

Acknowledgement: One of the authors (D.B.) gratefully acknowledges a fruitful discussion with Dr. K. Schindler on the subject of electrostatic subshocks.

References

Auer, P.L., H. Hurwitz, Jr., and R.W.Kilb
Large amplitude magnetic compression of a collision-free plasma, 2 Development of a thermalized plasma, Phys. Fluids 5, 298 (1962)

Auer, P.L., R.W. Kilb, and W.F. Crevier, Thermalization in the earth's bow shock, J. Geophys.Res. 76, 2927 (1971)

Bertotti, B., and D. Biskamp, Electrostatic instabilities in the earth's bow shock, Proceedings of a study group on collision free shocks held at ESRIN, Frascati ESRO Spec. Pap. SP-51, 41 (1969)

Bertotti,B., D. Parkinson, K. Schindler and P. Goldberg
ESRIN Internal Note No. 160 (1971)

Birdsall, C.K., and D. Fuss, Clouds-in-clouds, clouds-in-cells physics for many-body plasma simulation, J. Comp. Phys. 3, 494 (1969)

Forslund, D.W., and C.R.Shonk, Numerical simulation of electrostatic counterstreaming instabilities in ion beams, Phys. Rev. Lett. 25, 281 (1970)

Forslund, D.W., and J.P. Freidberg, Theory of laminar collisionless shocks, Phys. Rev.Lett. 27, 1189 (1971)

Forslund, D.W., R.L. Morse, and C.W. Nielson, Nonlinear electron-cyclotron drift instability and turbulence, Phys. Rev. Lett. 27, 1424 (1971)

Fredricks, R.W., C.F. Kennel, F.L. Scarf, G.W. Crook and I.M. Green, Detection of electric-field turbulence in the earth's bow shock, Phys.Rev.Lett. 21, 1761 (1968)

Fredricks, R.W., G.M. Crook, C.F. Kennel, I.M. Green, and F.L. Scarf, Ogo 5 observations of electrostatic turbulence in bow shock magnetic structures, J. Geophys. Res. 75, 3751 (1970)

Lindman, E.L., and W.E. Drummond, Studies of oblique shock structure, report of the University of Texas, Austin (1971)

Montgomery, M.D., J.R.Asbridge, and S.J. Bame, Vela 4 plasma observations near the earth's bow shock, J. Geophys. Res. 75, 1217 (1970)

Morse, R.L., and C.W. Nielson, Numerical simulation of warm two-beam plasmas, Phys.Fluids. 12, 2419 (1969)

Morse, R.L., Multidimensional plasma simulation by the particle-in-cell method, Methods in Computational Physics 9, 213 (1970)

Morse, R.L., and C.W. Nielson, Numerical simulation of the Weibel instability in one and two dimensions, Phys. Fluids 14, 830 (1971)

Papadopulos, K., R.C. Davidson, J.M. Dawson, I. Haber, D.A. Hammer, N.A. Krall, and R. Shanny, Heating of counterstreaming ion beams in an external magnetic field, Phys. Fluids 14, 849 (1971)

Papadopulos, K., C.G. Wagner, and I. Haber, High Mach-number turbulent magnetosonic shocks, Phys. Rev. Lett. 27, 982 (1971)

Rossow, V.J., Magnetic compression waves in collisionless plasma: Oblique ambient magnetic field, Phys.Fluids 10, 1056 (1967)

Tidman, D.A., The earth's bow shock wave, J. Geophys. Res. 72, 1799 (1967)

Wright, T.P., Instability of one-dimensional, oblique, magnetic shock structures, Phys.Fluids 14, 2337 (1971)

Figure Caption

Fig. 1 Coordinate system

Fig. 2 Ion x, v_x - phase space, magnetic field components B_y , B_z, total magnetic field B and electric potential ϕ of a magnetic shock at times a) $t = 1.25\,\Omega_i^{-1}$, b) $t = 3{,}25\,\Omega_i^{-1}$. Mass ratio is $\frac{mi}{me} = 128$.

Fig. 3 Ion x, v_x - phase space and magnetic field components B_y , B_z of a magnetic shock at $t = 2.25\,\Omega_i^{-1}$ for a) $\frac{mi}{me} = 64$, b) $\frac{mi}{me} = 128$, c) $\frac{mi}{me} = 256$. The ions are unmagnetized here.

Fig. 4 High resolution ion phase space plots showing the existence of small scale electrostatic turbulence taken at $t = 1.5\,\Omega_i^{-1}$, with the parameters of the run shown in Fig 2., except $T_i = 0.01$ so that $T_e/T_i = 25$.

Fig. 5 Ion phase space plots of the 2-ion beam instability

a) linear instability at t = o and $t = 40\ \omega_{pi}^{-1}$ for $u = \pm\ 0.75\,c_s$

b) For $U = \pm\ 3\,c_s$ and initial perturbation $e\phi_o = 0.25\ T_e$ no instability develops (plots taken at t = o and $t = 80\ \omega_{pi}^{-1}$)

c) nonlinear instability for $u = \pm\ 3$ and $e\phi_o = 0.5\ T_e$ (as in b) plots taken at t = o and $t = 80\ \omega_{pi}^{-1}$)

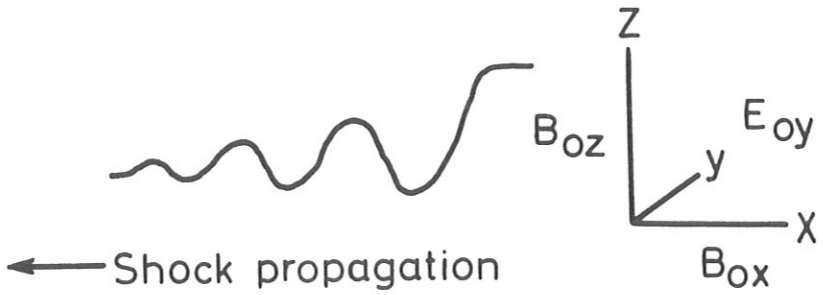

Fig.1

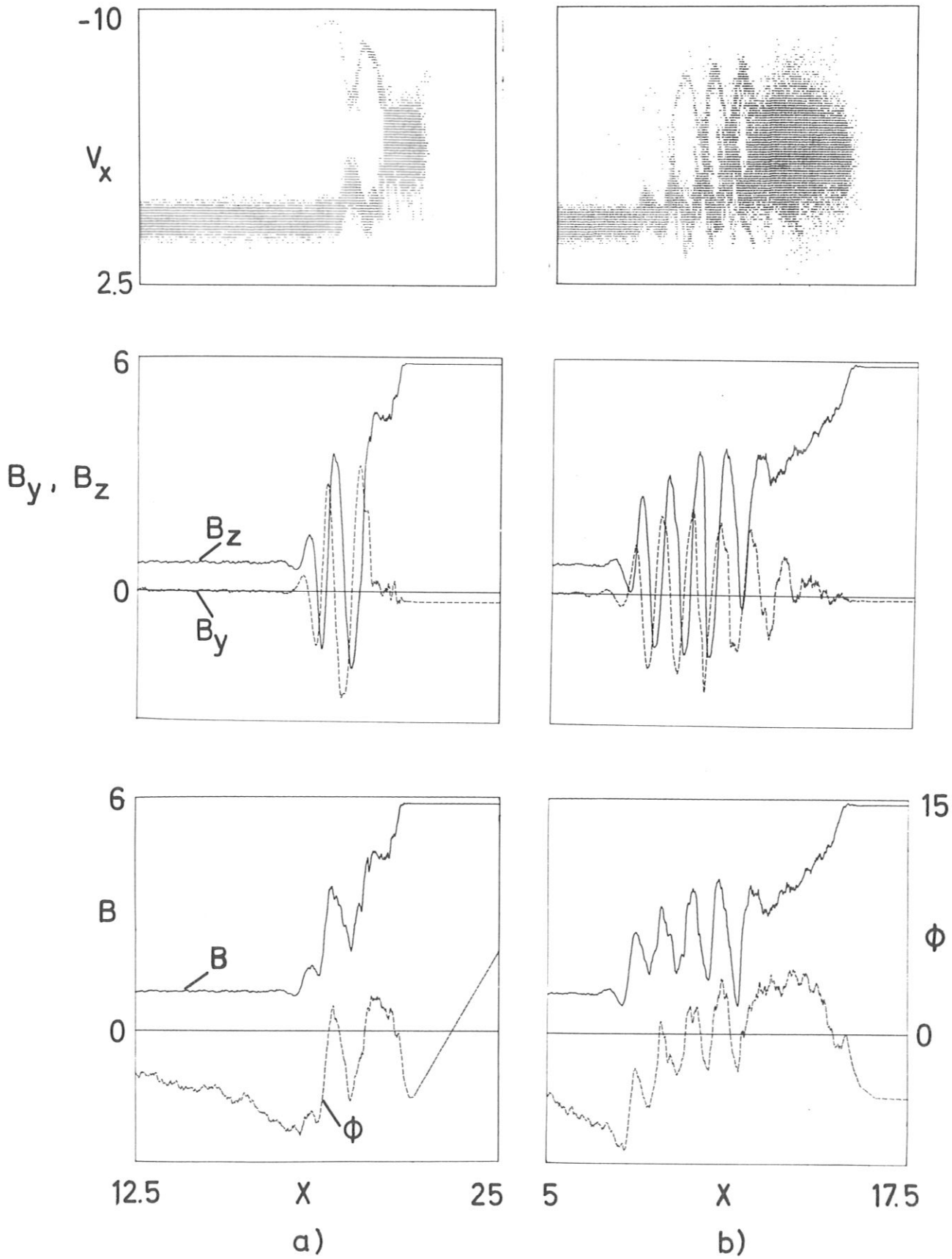

Fig. 2

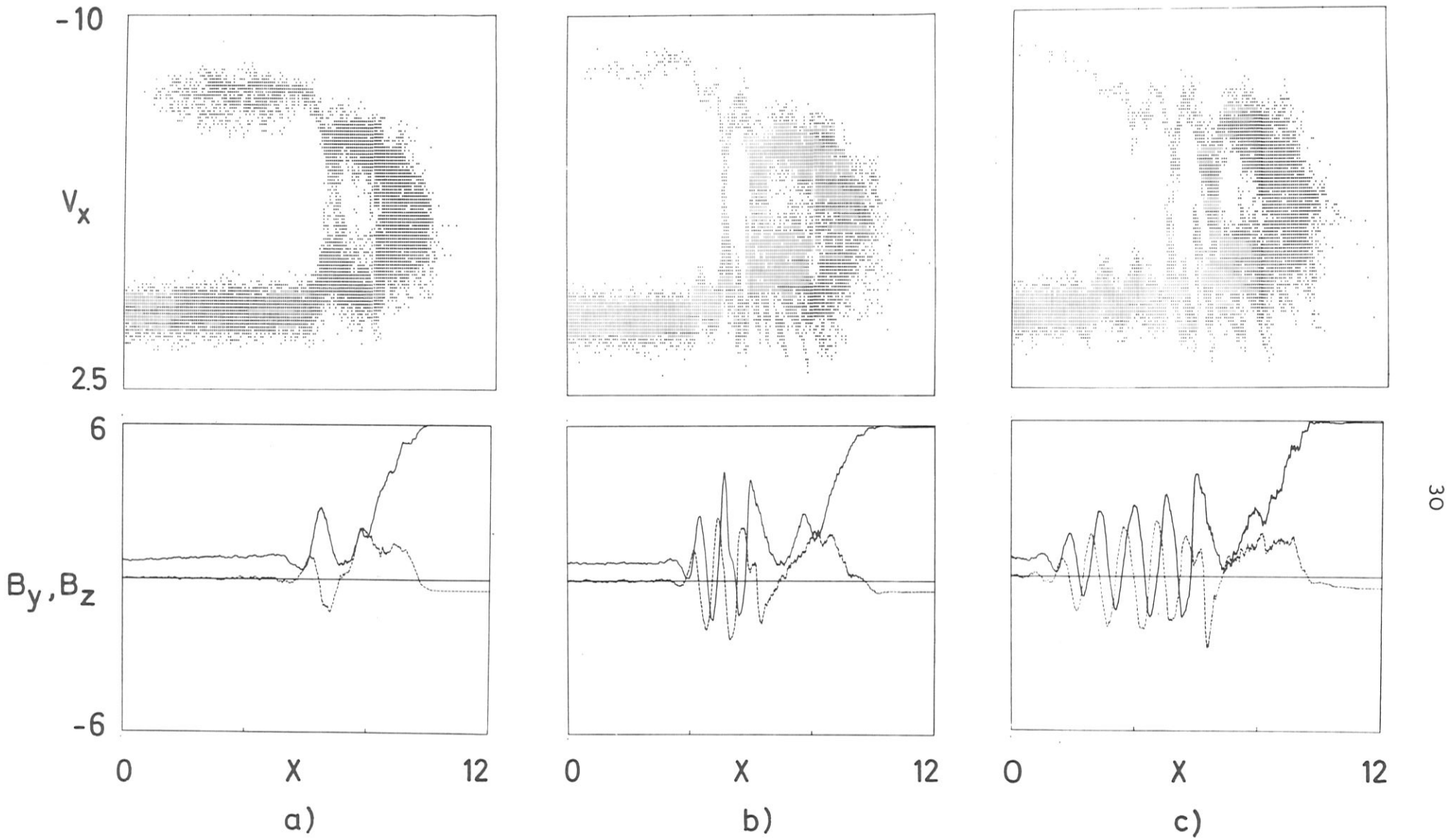

Fig. 3

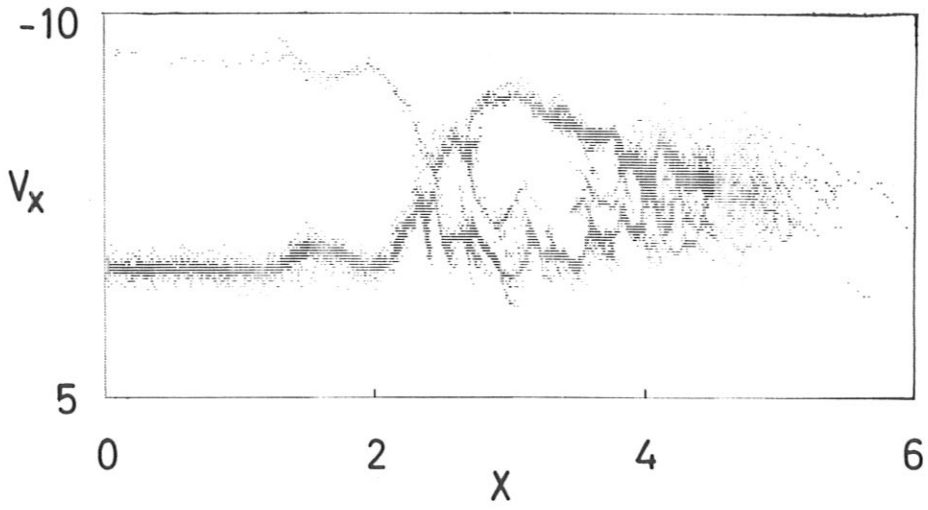

Fig. 4

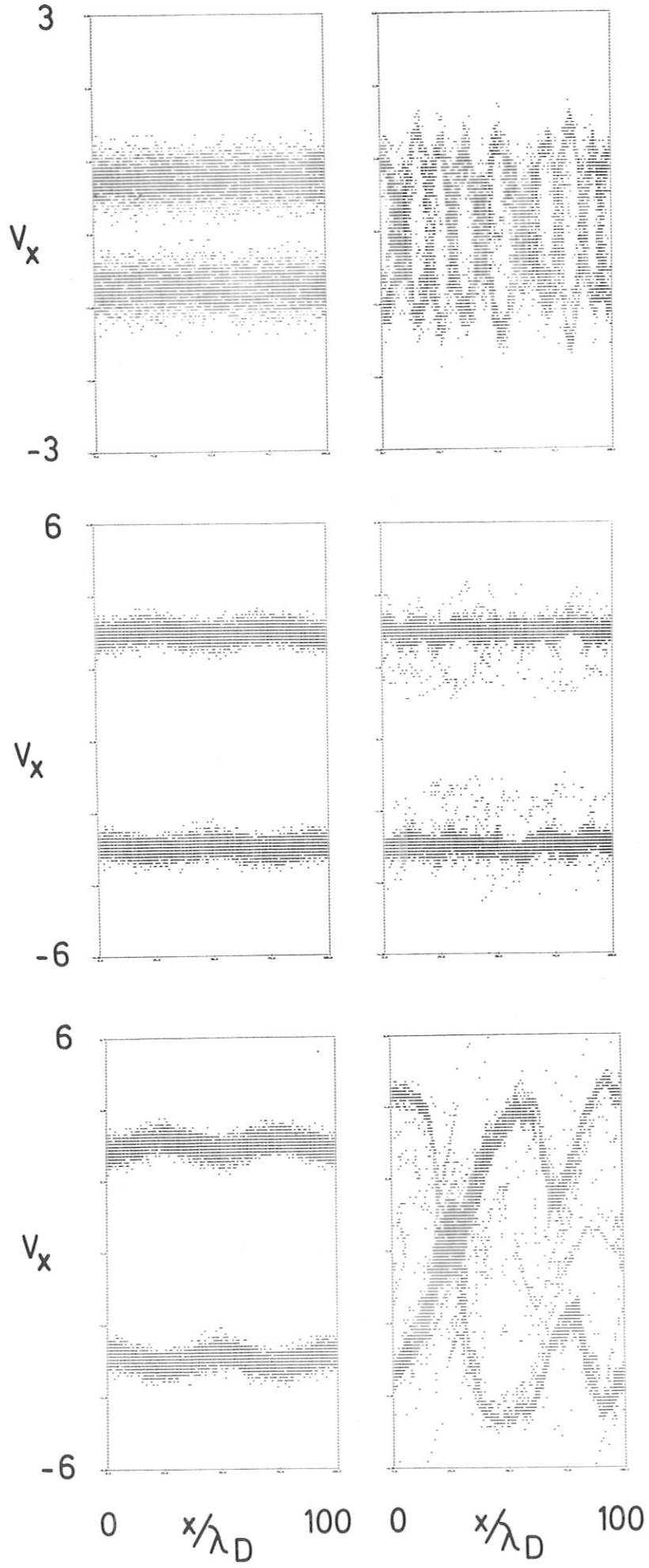

Fig.5